Absolute rate coefficients for dielectronic recombination of Na-like Kr²⁵⁺

Z. K. Huang,[1] W. Q. Wen,[1,2,*] S. X. Wang,[3] N. Khan,[1,2] H. B. Wang,[1] C. Y. Chen,[4] C. Y. Zhang,[4] S. P. Preval,[5] N. R. Badnell,[6]
W. L. Ma,[3] X. Liu,[1] D. Y. Chen,[1] X. L. Zhu,[1,2] D. M. Zhao,[1] L. J. Mao,[1,2] X. M. Ma,[1] J. Li,[1] M. T. Tang,[1] R. S. Mao,[1,2]
D. Y. Yin,[1] W. Q. Yang,[1] J. C. Yang,[1,2] Y. J. Yuan,[1,2] L. F. Zhu,[3] and X. Ma [1,2,7,†]

[1]*Institute of Modern Physics, Chinese Academy of Sciences, 730000, Lanzhou, China*
[2]*University of Chinese Academy of Sciences, 100049, Beijing, China*
[3]*Hefei National Laboratory for Physical Sciences at Microscale, Department of Modern Physics, University of Science*
and Technology of China, 230026, Hefei, China
[4]*Shanghai EBIT Laboratory, Institute of Modern Physics, Fudan University, and the Key Laboratory of Applied Ion Beam Physics,*
Chinese Ministry of Education, Shanghai 200433, China
[5]*Department of Physics and Astronomy, University of Leicester, Leicester, LE1 7RH, United Kingdom*
[6]*Department of Physics, University of Strathclyde, Glasgow G4 0NG, United Kingdom*
[7]*ExtreMe Matter Institute EMMI, GSI Helmholtzzentrum für Schwerionenforschung, 64291, Darmstadt, Germany*

The absolute rate coefficients for dielectronic recombination (DR) of sodiumlike krypton ions were measured by employing the electron-ion merged-beam technique at the heavy-ion storage ring CSRm at the Institute of Modern Physics in Lanzhou, China. The measured DR spectrum covers the electron-ion collision energy range of 0–70 eV, encompassing all of the DR resonances due to $3s \to 3p$ and part of the DR resonances from $3s \to 3d(\Delta n = 0)$ and $3s \to 4l(\Delta n = 1)$ core excitations. A series of peaks associated with DR processes have been identified by the Rydberg formula. The experimental DR results are compared with the theoretical calculations using a relativistic configuration interaction flexible atomic code and the distorted-wave collision package AUTOSTRUCTURE. A very good agreement has been achieved between the experimental results and the theoretical calculations by considering the strong mixing among the low-energy resonances in both calculations. The experimentally derived DR spectrum is then convolved with a Maxwellian-Boltzmann distribution to obtain the temperature dependent plasma recombination rate coefficients and compared with previously available results from the literature. The present experimental result yields a precise plasma rate coefficients at the low temperature range up to $\sim 1 \times 10^6$ K and the calculated data by Altun *et al.* [Z. Altun, A. Yumak, N. R. Badnell, S. D. Loch, and M. S. Pindzola, Astron. Astrophys. **447**, 1165 (2006)] provide reliable plasma rate coefficients at high temperature range above 2×10^6 K.

I. INTRODUCTION

Dielectronic recombination (DR) is a basic electron-ion recombination mechanism, which is a two-step resonant process and can be explained as the combination of dielectronic capture and radiative stabilization [1–3]. The first step is associated with the simultaneous capture of a free electron into some bound states and the excitation of a bound electron forming an intermediate doubly excited state. In the second step, the resulting doubly excited state decays radiatively to states below the autoionization threshold. Thus, DR is important for studying the structure, formation, and decay of doubly excited states, which requires a full consideration of electron correlation in order to model them accurately [4]. The precision DR spectroscopy of highly charged ions has already been employed to investigate the strong-field quantum electrodynamics effects, electron-electron interaction, as well as relativistic effect [5–7]. Additionally, electron-ion re-

combination rate coefficients are essential for determining the level populations and the ionization balance in a coronal and dense plasmas, like, e.g., laser produced plasmas (optical and X-ray free electron laser) [3,8–11], fusion plasmas [12,13]. The reliable DR rate coefficients are crucial for understanding the properties of fusion and astrophysical plasmas, including charge state distribution, thermal structure and elemental abundances [14–16]. However, it is still challenging to calculate the DR resonance positions and strengths of multi–electron ions with sufficient precision by using the presently available theoretical atomic structure code, particularly at low electron–ion collision energies. Because an infinite number of states are involved in the DR process of highly charged ions and relativistic many-body effects should be considered with high orders in the theoretical calculations. The measurements of electron-ion recombination rate coefficients with high accuracy are required to benchmark different theoretical methods and to produce more reliable data for use in plasma modeling.

A storage ring equipped with an electron cooler provides a uniquely effective technique to determine accurate and absolute DR rate coefficients, especially at the low energy

---

*Corresponding author: wenweiqiang@impcas.ac.cn
†Corresponding author: x.ma@impcas.ac.cn

electron-ion collisions. A series of DR experiments with highly charged ions have been carried out at the storage rings, i.e., TSR at MPIK in Heidelberg [17], ESR at GSI in Darmstadt [18], CRYRING at MSL in Stockholm [19], and CSRm at the Institute of Modern Physics (IMP) in Lanzhou [20]. More details about DR experiments at the storage rings can be found in recent reviews [4,17,21], and the references therein.

Krypton has already been used as an injected impurity gas for diagnostics in tokamak fusion plasmas [22]. It has recently been proposed to use the *K*-shell emission of krypton ions to diagnose the initial ITER (International Thermonuclear Experimental Reactor) plasmas by using the x-ray imaging spectrometer system [23]. In order to analyze the observed emission lines from the ionized krypton ions in fusion plasmas and astrophysical plasmas, the accurate atomic parameters including excitation energies, ionization rate, and recombination rates are needed and have already been widely investigated by many different theories. A summary of krypton transitions and energy levels is listed in a review by Saloman in Ref. [24]. For Na-like ions, these one-active-electron systems usually produce strong and well-isolated spectral lines which are well suited for experimental measurement, and these data are essentially needed in many specific applications. Due to their relatively simple electronic structure, precision spectroscopy of Na-like ions is also essentially important for testing the reliability of atomic structure calculations. Previous DR experiments with several Na-like ions have been performed at heavy-ion storage rings, i.e., Si^{3+} [25], S^{5+} [26], Ar^{7+} [26], Fe^{15+} [27], and Ni^{17+} [28,29], to not only provide accurate recombination rate coefficients for plasma modeling, but also test the theoretical methods.

Here, we present the absolute electron-ion recombination rate coefficients of Na-like krypton from an experiment at the storage ring CSRm as well as the theoretical calculations using the AUTOSTRUCTURE code and flexible atomic code (FAC) code. The measured spectrum covers the electron-ion collision energy from 0 to 70 eV, which includes the radiative recombination (RR) and DR processes and the most significant recombination channels can be expressed as

$$Kr^{25+}(3s[^2S_{1/2}]) + e^- \rightarrow$$

$$\begin{cases} Kr^{24+}(3s[^2S_{1/2}]nl) + h\nu, RR \\ Kr^{24+}(3p[^2P_{1/2,3/2}]nl)^{**}(n \geqslant 13) \rightarrow Kr^{24+} + h\nu, DR \\ Kr^{24+}(3d[^2D_{3/2,5/2}]nl)^{**}(n \geqslant 8) \rightarrow Kr^{24+} + h\nu, DR \\ Kr^{24+}(4l4l')^{**} \rightarrow Kr^{24+} + h\nu, DR, \end{cases}$$

$$(1)$$

where $h\nu$ denotes the decay photons, and n is the principal quantum number of the captured electron. The transition energies associated with the DR channels including $3s \rightarrow 3p$ and $3s \rightarrow 3d(\Delta n = 0)$ and $3s \rightarrow 4l(\Delta n = 1)$ are listed in Table I. The associated core excitation energies for $3s[^2S_{1/2}] \rightarrow 3p[^2P_{1/2}]$ and $3s[^2S_{1/2}] \rightarrow 3p[^2P_{3/2}]$ are 56.340 eV and 69.267 eV, respectively [24]. These two channels involve the excitation of a 3s electron to the 3p level and all the associated DR resonances have been observed within the present measured energy range. However, the core excitation energy for $3s[^2S_{1/2}] \rightarrow 3d[^2D_{3/2}]$ and $3s[^2S_{1/2}] \rightarrow 3d[^2D_{5/2}]$ are 144.340 eV and 146.796 eV, respectively [24], and the

TABLE I. Energy levels for Na-like Kr^{25+} ions.

Level configuration	Excitation energy(eV)[a]
$1s^22s^22p^63s[^2S_{1/2}]$	0
$1s^22s^22p^63p[^2P_{1/2}]$	56.340
$1s^22s^22p^63p[^2P_{3/2}]$	69.267
$1s^22s^22p^63d[^2D_{3/2}]$	144.340
$1s^22s^22p^63d[^2D_{5/2}]$	146.796
$1s^22s^22p^64s[^2S_{1/2}]$	557.147
$1s^22s^22p^64p[^2P_{1/2}]$	580.175
$1s^22s^22p^64p[^2P_{3/2}]$	585.285
$1s^22s^22p^64d[^2D_{3/2}]$	613.368
$1s^22s^22p^64d[^2D_{5/2}]$	614.463
$1s^22s^22p^64f[^2F_{5/2}]$	628.266
$1s^22s^22p^64f[^2F_{7/2}]$	628.708

[a]Energy levels taken from NIST atomic spectra database [24].

series limits, except several discrete resonances, of these two channels cannot be observed in the measured spectra. In addition to $\Delta n = 0$ core excitations, DR resonances associated with $3s \rightarrow 4l(\Delta n = 1)$ core excitations have also strongly contributed to the measured DR spectra.

In order to fully understand the measured electron-ion recombination spectrum of sodiumlike Kr^{25+}, the theoretical calculations of DR rate coefficients were performed using the updated atomic package of FAC (version 1.1.4) [30,31] and AUTOSTRUCTURE code [32,33] to compare with the experimental results. A very good agreement between the experimental results and the theoretical calculations has been achieved by considering the strong mixing for low energy DR resonances in both calculations. It should be noted that the plasma rate coefficients of Kr^{25+} have already been calculated by using the AUTOSTRUCTURE from Altun *et al.* (2006) [34]. However, since they calculated the $\Delta n = 0$ and $\Delta n = 1$ core excitations separately, there was no mixing between the low-lying resonances arising from the separate core excitations. The present AUTOSTRUCTURE calculations include the necessary mixing and better agreement (within experimental uncertainty) is found with the measured result at low energies. Therefore, our results provide benchmark recombination data of Kr^{25+} for testing atomic theory and for plasma modeling in astrophysics and fusion science in the low temperature up to medium temperature regime.

The paper is organized as follows: Sec. II gives a brief description of the present theoretical methods. In Sec. III, the experimental method and the basic data analysis are introduced. In Sec. IV, the experimental results, including the measured electron-ion recombination rate coefficients as well as the derived plasma recombination rate coefficients are presented and discussed. Finally, we summarize the results as a conclusion in Sec. V.

II. THEORY

The detailed descriptions of the theoretical methods of FAC code and AUTOSTRUCTURE can be found in the reference of Gu *et al.* [30,31] and Badnell *et al.* [32], respectively. Here, we will only briefly describe these calculation procedures and their updates. For the FAC calculation, DR resonance strengths

were calculated using the isolated resonance approximation with the distorted-wave method based on the Dirac equation. Atomic energy levels, autoionization and radiative decay rates were calculated with a relativistic atomic-structure program. During the calculation, the resonance energies were empirically adjusted with the core excitation energies available from the NIST atomic database [24]. Such adjustments are necessary to obtain more reliable low-lying DR resonances in the calculations.

The DR process was treated as two independent steps in the calculations. The first step is dielectronic capture (DC), which is the time inversal of autoionization (AI) process. In the second step, the doubly excited intermediate states can either autoionize or decay radiatively thereby completing the DR process. Accordingly, the DR cross section via a specific doubly excited state is the product of the DC cross section and the branching ratio of radiative stabilization. DC cross section can be obtained from the AI rates through the principle of detailed balance and its strength can be written as

$$S_{DC} = \frac{g_i}{2g_f} \frac{\pi^2}{E_c} A^a, \qquad (2)$$

where g_i and g_f are the statistical weights of the initial state and final autoionizing state after DC, respectively, E_c is the electron collision energy and A^a is the AI strength. A zero-density approximation radiative branching ratio can be expressed as

$$B(i) = \frac{\sum_k A_{ik}^r}{\sum_h A_{ih}^r + \sum_m A_{im}^a}, \qquad (3)$$

where A_{ih}^r denotes the radiative decay rate from state i to h and A_{im}^a denotes the autoionization rate, h and m represent the levels below the ionization threshold and those after ionization, respectively [30,35]. In the present FAC calculation of DR process of Na-like Kr^{25+}, to reproduce accurately enough the positions of the low-energy resonances, the second-order relativistic many-body perturbation theory implemented within FAC is employed to calculate the energies for levels arising from $3lnl'$ with $n \leqslant 9$ and $l' \leqslant 8$ and $4l4l'$ configurations in Mg-like Kr^{24+}. The detailed calculation is similar to those performed for non-autoionizing levels in Cu^{17+} [36] and Kr^{24+} [37]. The configuration-interaction (CI) between the $3lnl'$ and $4lnl'$ configurations with $n \leqslant 9$ has been considered in the calculations for autoionizing and radiative transition rates. The energies for the $n > 9$ resonances are empirically corrected using the experimental excitation energies via Rydberg formula. These high-lying resonances are considered using the hydrogenic scaling laws of Auger and radiative transition rates.

For AUTOSTRUCTURE calculation, the underlying theoretical method implemented is well documented. For a target ion $X_v^{(Q)}$ with a residual charge Q and initial state v, colliding with an electron and recombining into an ion $X_f^{(Q-1)}$ with final state f, the partial DR cross section σ_{fv}^Q, energy averaged over a bin width ΔE_c, can be expressed as

$$\sigma_{fv}^Q(E_c) = \frac{(2\pi a_0 I_H)^2 \tau_0}{E_c} \sum_j \frac{g_j}{2g_i} \frac{\sum_l A_{j \to i, E_c l}^a A_{j \to f}^r}{\sum_h A_{j \to h}^r + \sum_{m,l} A_{j \to m, E_c l}^a}, \qquad (4)$$

where $E_c{}^l$ is the energy of the continuum electron with angular momentum l, fixed by the position of the resonances. I_H is the ionization energy of the hydrogen atom. $(2\pi a_0)^2 \tau_0 = 2.6741 \times 10^{-32}$ cm^{2}s. The sum over l covers the angular momentum quantum numbers of the Rydberg electron. The sum over j covers all autoionization states. Lastly, the sum over h and m represents the total radiative and autoionization widths, respectively. In the AUTOSTRUCTURE calculation for the DR process of Na-like Kr^{25+} in the present work, for $\Delta n = 0$ core excitations, the resonance energies are empirically adjusted so that the series limits match the $3 \to 3$ core excitation energies obtained from the NIST database. In this case ($\Delta n = 0$), l and n values were included up to 18 and 25, respectively, and a quantum-defect theoretical approximation for high-level values of n up to 1000 was used [38]. For $3 \to 4$ ($\Delta n = 1$) core excitations, l and n values were included up to 7 and 25, respectively. The detailed comparison for calculation of DR cross sections between AUTOSTRUCTURE and FAC codes are described in Refs. [39,40].

In order to compare with the experimentally derived electron-ion recombination rate coefficients, the calculated electron-ion recombination cross sections have to be transformed into the rate coefficients according to the following formula:

$$\alpha(E) = \int_{-\infty}^{+\infty} \sigma(v) v f(v, T_\parallel, T_\perp) d^3 v, \qquad (5)$$

where $f(v, T_\parallel, T_\perp)$ is the anisotropic velocity distribution function of electron beam. The characteristic parallel component $T_\parallel$ and perpendicular component $T_\perp$ of electron temperatures distribution with respect to the propagation direction of the electron beam were obtained by fitting the low energy spectrum with a flattened Maxwellian profile [41].

III. EXPERIMENT AND DATA ANALYSIS

Measurements of the electron-ion recombination rate coefficients were performed at the main cooler storage ring (CSRm) at IMP in Lanzhou, China. A detailed description of the experimental setup and method can be found in the literature [42,43]. Here, we will only briefly describe the electron-ion recombination experiment of sodiumlike Kr^{25+} at the CSRm. Beam of sodiumlike Kr^{25+} ions was first produced in the Electron Cyclotron Resonance ion source [44], accelerated to a beam energy of 4.98 MeV/u in the Sector Focused Cyclotron, and then injected into and accumulated in the CSRm. The typical beam current, measured with a DC current transformer (DCCT), was about 200 μA, corresponding to 2.6×10^8 ions being stored in the CSRm. The lifetime of ion beams was estimated to be ~120 s. During the measurement, the electron and ion beams were merged over an effective interaction length of $L = 4.0$ m in the straight section of the cooler. In order to generate a colder electron beam and realize a higher experimental energy resolution, the electron beam was adiabatically expanded from the magnetic field of $B = 125$ mT at the electron-gun section to 39 mT at the electron-cooling section. The resulting electron beam diameter was constrained to 52 mm at the cooling section, with a typical electron density of 3.85×10^5 cm^{-3}. The electron beam was also utilized as an electron target in the

DR experiment. After the injected ions were cooled with the velocity matched electron beam for several seconds, the detuning system loaded an offset voltage to the cathode HV to scan the electron beam energy according to a preset timing sequence. Generally, a measurement cycle covers a series of different detuning voltages with an equidistant minimum step of 1 volt in the laboratory system. The detuning timing sequence is set for energy detuning for 10 ms and for electron cooling for 190 ms for each single detuning voltage [20]. This provided nonzero relative energies between electron and ion beams in the center-of-mass frame. Downstream of the cooler, the recombined ions were separated from the primary ion beam in the first bending magnet and detected by a movable scintillator particle detector with nearly 100% efficiency [45]. In the whole measurement, DCCT was used to monitor the ion beam current in real time. Ion and electron beam position monitors were utilized to monitor the relative positions of the ion beam and the electron beam in the straight section of the cooler. All the DR measurements were performed under the condition of keeping the electron beam and ion beam parallel along the axis of the cooler. In addition, a Schottky pick-up was employed to monitor the revolution frequency and the momentum spread of the ion beam [46]. In this work, the momentum spread $\Delta p/p$ of the ion beam was estimated to be 2.13×10^{-4}.

The relative energy between electron and ion beams in the center of mass frame was calculated with the following formula:

$$E_{\rm rel} = \sqrt{m_e^2 c^4 + m_i^2 c^4 + 2m_e m_i \gamma_e \gamma_i c^4 (1 - \beta_e \beta_i \cos\theta)} - m_e c^2 - m_i c^2, \tag{6}$$

where m_e and m_i are the electron and ion rest mass, respectively. c is the speed of light, γ_e and γ_i denote the Lorentz factors of electron and ion beams, respectively. The angle θ between electron and ion beam is safely considered as zero in the present experiment. Space charge effects were carefully considered and the drag force effects were found to be negligible.

For electron-ion recombination experiments at heavy ion storage rings, the recombination rate coefficients α can be deduced from the recombination counting rate R at a relative energy $E_{\rm rel}$ between electron and ion by [7]

$$\alpha(E) = \frac{R(E)}{N_i n_e (1 - \beta_i \beta_e)} \frac{C}{L}. \tag{7}$$

Here, the counting rate R includes DR, RR and the background rate from collision of the ions with residual gas, where N_i is the number of the stored ions, n_e is the density of electron beam, $v_e = \beta_e c$ and $v_{\rm ion} = \beta_i c$ are the velocities of electron beam and ion beam, L is length of the effective interaction section, and C is the circumference of the storage ring. In order to compare the measured DR rate coefficient with the theoretical ones, we subtracted background from measured rate coefficients using an empirical background function: $\alpha_{RR+BG}(E_{\rm rel}) = \alpha_0 + \alpha_1 E_{\rm rel} + \frac{\alpha_2}{1 + \alpha_3 E_{\rm rel} + \alpha_4 E_{\rm rel}^2}$, with the α_i determined by fitting these parts of the spectrum that do not exhibit DR resonances. In order to make sure that the subtraction of the RR contribution is correct, the RR rate coefficient was
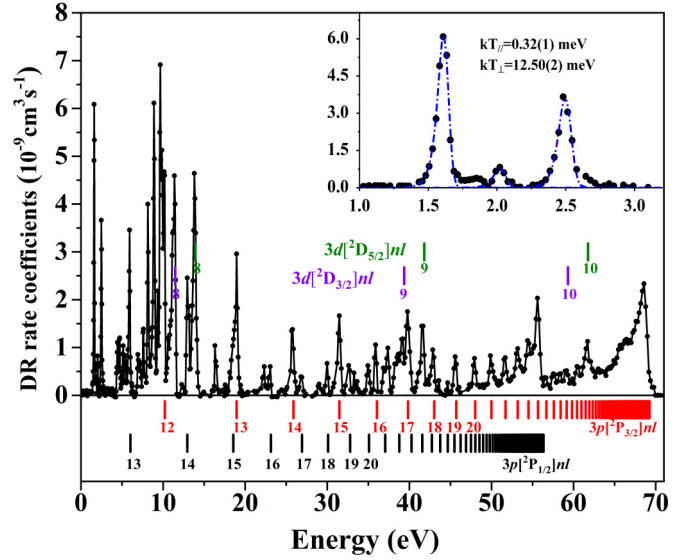

FIG. 1. Electron-ion recombination rate coefficients of sodium-like krypton as a function of collision energy. The energy scale of the experimental spectra (black connected filled circles) was recalibrated by a factor of 1.022 to achieve agreement with the $3p[^2P_{3/2}]nl$ series limit at 69.267 eV. The electron temperatures of the electron beam were $k_B T_\parallel = 0.32(1)$ meV and $k_B T_\perp = 12.50(2)$ meV in longitudinal and transversal directions, respectively.

also calculated for a cross check by a modified version of the semiclassical Bethe and Salpeter formula for hydrogenic ions [47]. The calculated RR contribution by the formula of Bethe and Salpeter agrees very well with the fitted background from an empirical function, but shows a significant difference at an energy range below 0.8 eV, the deviations below 0.8 eV are smooth and do not indicate further low-lying DR. However, the deviations from the hydrogenic RR model have a different behavior than that shown in Ref. [48]. While the origin of this discrepancy remains unclear, there is no indication that the measured smooth rate should be not attributed to DR. Hence, it can be subtracted using a fitted empirical curve.

Energy dependent DR rate coefficients of Kr^{25+} were investigated in the energy range up to 70 eV, constituting all $\Delta n = 0$ DR resonances up to the $3s_{1/2} \to 3p_{1/2}$ and $3s_{1/2} \to 3p_{3/2}$ series limit. The systematic corrections for space charge effects were processed in the usual manner [20,49]. The predominant uncertainty of the rate coefficients measured in this work is estimated to be about 30% at a 1σ confidence level, including a 1% uncertainty for statistics, a 10% uncertainty for the electron and ion beam current and the electron-ion interaction length, an uncertainty of 15% due to the background subtraction and an uncertainty of 25% for the electron density in the cooler section and the position of the ion beam in this profile.

IV. RESULTS AND DISCUSSION

A. Merged-beam DR rate coefficients

Figure 1 depicts the measured DR rate coefficients of Na-like Kr^{25+} over the energy range of 0–70 eV. The Rydberg series of $2p^63p[^2P_{1/2}]nl$ DR resonances also converges to

their series limits at 56.340 eV. The $3p$ fine structure splitting of 12.936 eV is clearly resolved. In addition, part of the $2p^6 3dnl$ ($n = 8, 9, 10$) resonances associated with the $3s \rightarrow 3d$ core excitation also appeared in the measured energy range.

In the DR spectrum, the position of each Rydberg resonance can be well estimated from the hydrogenic Rydberg formula for the high-n values:

$$E_{\text{res}}(n) = E_{\text{exc}} - R_y \frac{q^2}{(n - \delta)^2}, \qquad (8)$$

with the Rydberg constant $R_y = 13.60569$ and charge state $q = 25$ of the initial ion beam. n denotes the principal quantum number of the captured electron and E_{exc} is the core excitation energy. It should be noted that the formula is inadequate for low n levels where fine structure dominate the DR resonance structure. As presented in Fig. 1, the minimum principal quantum numbers for DR process via $3s[^2S_{1/2}] \rightarrow 3p[^2P_{1/2}]$, $3p[^2P_{3/2}]$, $3d[^2D_{3/2}]$ and $3d[^2D_{5/2}]$ core excitations are 13, 12, 8, and 8, respectively. The positions for each Rydberg series of the intermediate levels of $3p[^2P_{1/2}]nl$ ($n \geqslant 13$), $3p[^2P_{3/2}]nl$ ($n \geqslant 12$), and $3d[^2D_{3/2,5/2}]nl$ ($n \geqslant 8$) are indicated with vertical bars in different colors. It can be seen that the series limits for $3p[^2P_{1/2,3/2}]nl$ can be observed around 56 eV and 69 eV. Since the core excitation energies for $3s[^2S_{1/2}] \rightarrow 3d[^2D_{3/2}]$ and $3d[^2D_{5/2}]$ are 144.340 and 146.796 eV, their series limits cannot be observed within the energy range of measured spectrum. In Fig. 1 and throughout the paper, we have adjusted the collision energy scale by multiplying it with a constant factor 1.022, which brings the series limit of $3p[^2P_{3/2}]nl$ into agreement with the spectroscopic value of 69.267 eV. After this correction, we have a very good agreement between the experimental results and the theoretical calculations at isolated high n DR resonance and also the positions of the series limit. The error bar for the scale factor is determined as 1.022 ± 0.004.

In the storage ring DR measurement, the charge-changed recombined ions experience magnetic fields on the travel from the electron cooler to the detector. Along the ion trajectory, the magnetic fields range from 0.039 T in the toroidal coils of the electron cooler to the 0.185 T in the dipole bending magnets. The motional electric fields produced therein are sufficient to reionize the loosely bound high Rydberg electron in the recombined ions. With these electric fields, the principal quantum state cutoff for the field ionization is determined by [50]

$$n_{\text{cutoff}} \simeq \left[6.2 \times 10^8 \left(\frac{V}{cm} \right) \frac{q^3}{v_i \times B} \right]^{1/4} \qquad (9)$$

where q is the charge state of the initial ion, v_i is the mean velocity of ion beam, and B is the magnetic field strength of the dipole magnet before the detection of recombined ions. The field-ionization n_{cutoff} effect can be seen at the series limits of $3p[^2P_{1/2}]nl$ and $3p[^2P_{3/2}]nl$ around 56 and 69 eV in Fig. 3. The field-ionized ions cannot be separated from the primary ion beam and result in a reduced counting rate of recombined ions. As a result, only dielectronic capture into Rydberg levels with $n < n_{\text{cutoff}}$ will contribute to the recombination counting rates in the experiment. In order to obtain an
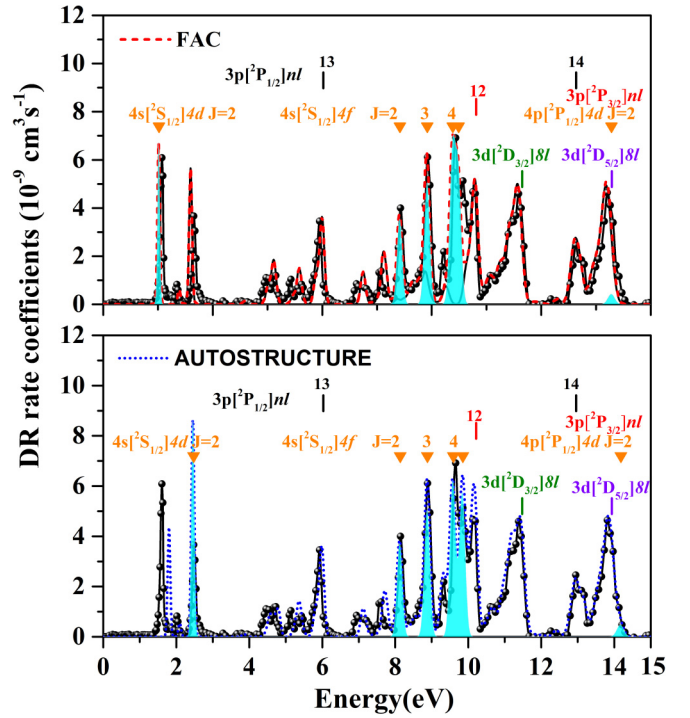

FIG. 2. Detailed comparison between the FAC code (upper panel) and AUTOSTRUCTURE (lower panel) calculated and measured DR rate coefficients of Na-like Kr^{25+} within the energy rage of 0–15 eV. The connected black circles are the measured DR spectrum with background subtracted. The dashed red and shot-dotted blue curves are the FAC and AUTOSTRUCTURE calculated total DR rate coefficient with n up to 300 and 1000 in each panel, respectively. The cyan areas give the DR rate coefficient associated with $3l \rightarrow 4l (\Delta n = 1)$ core excitation.

appropriate cutoff number, we have varied the value of n_{cutoff} in the FAC calculations to achieve a good agreement with the measured DR rate coefficients around the series limit of $3p$, as shown in Fig. 3, and the estimated $n_{\text{cutoff}} = 150$ in the present experiment.

In order to obtain the characteristic parallel and perpendicular electron temperatures, the low energy DR spectrum was fitted as shown in the inset of Fig. 1. The fitting function is a δ function convolved with a flattened Maxwellian distribution characterized by the anisotropic electron temperatures $T_{\|}$ and $T_{\perp}$ in longitudinal and transversal directions [41]. With respect to the electron beam propagation direction, the obtained longitudinal and transversal temperatures of electron beam were $k_B T_{\|} = 0.32(1)$ meV and $k_B T_{\perp} = 12.50(2)$ meV, respectively. The numbers in brackets correspond to the uncertainties from the fit with one standard deviation.

An essential convolution of the fitted electron beam velocity distribution with the calculated DR cross sections by FAC and AUTOSTRUCTURE, as described in Sec. II, was made to derive the theoretical rate coefficients, and compare with the experimentally measured results. Figures 2 and 3 present the detailed comparison between the measured DR rate coefficients and the theoretical calculations of FAC code and AUTOSTRUCTURE over the energy rage of 0–15 eV and 35–70 eV, respectively. Since the first DR resonance
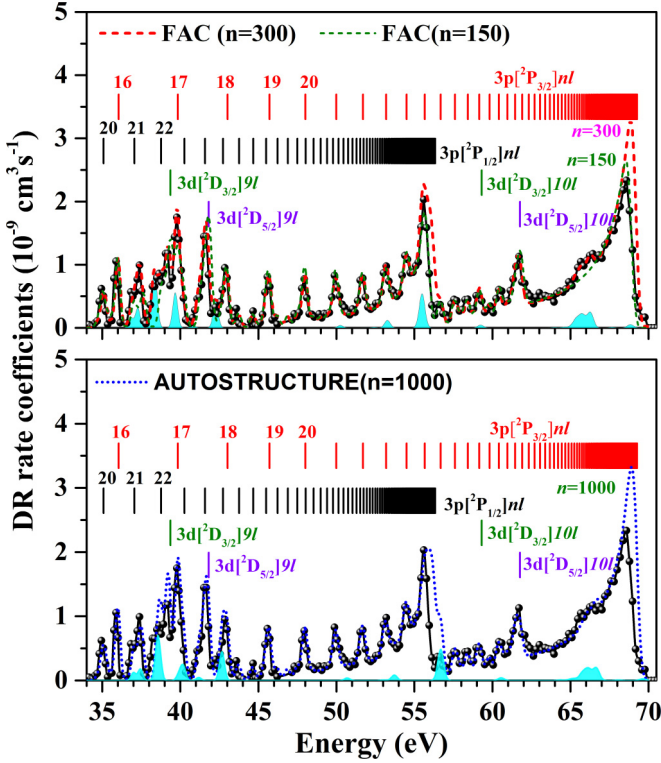
FIG. 3. Same as Fig. 2, but for the energy rage of 35–70 eV. The field-ionization effect appeared at the series limits of $3p[^2P_{1/2}]nl$ and $3p[^2P_{3/2}]nl$ around 56 eV and 69 eV, respectively. The dashed olive and dashed red curves are the FAC calculation in which the field ionization effect was considered with $n_{\text{cut-off}} = 150$ and 300, respectively. The shot-dotted blue curve is the AUTOSTRUCTURE calculated DR spectrum with $n_{\text{max}} = 1000$.

peak appears around 1.5 eV for Kr^{25+}, which is already far off the RR rate coefficient enhancement region, the RR rate enhancement will have minor impact on our results and the contribution from RR and background can be fully removed with optimized data analysis [48,51], as shown in Fig. 2. In addition to $\Delta n = 0$ core excitation, the DR resonances associated with $3s \rightarrow 4l(\Delta n = 1)$ core excitations were found strongly contributing to the measured spectrum, see the cyan areas in Figs. 2 and 3. However, the calculations on the DR resonance associated with $3s \rightarrow 4l(\Delta n = 1)$ core excitations are very difficult. One reason is that there is no reference energy levels available for the autoionization states $4l4l'$ of Mg-like ions except for the x-ray spectra of Mg-like Zn [52]. Another reason is that the electron-electron correlation effects should be treated carefully in the calculations for these strongly correlated intermediate states.

The comparison of FAC calculation with the experimental result in the energy range of 0–15 eV is presented in the upper panel of Fig. 2, the resonance positions and strengths are well reproduced by the present FAC calculation. However, the resonances at 1.619 and 2.500 eV in the measured spectrum show differences of 90 and 100 meV from the FAC calculated values of 1.530 and 2.405 eV, respectively. The differences in resonance energies will result in an obvious difference between the

experimentally derived plasma rate coefficients and FAC data, which will be discussed in Sec. IV. It should be noted that the mixing among the low-energy resonances is very strong. For example, the dominant components in the wave functions of the two resonances mentioned above are $-0.762[3d_{3/2}8s]_2 - 0.413[4s4d_{5/2}]_2$ and $-0.641[3d_{3/2}8s]_2 + 0.428[4s4d_{5/2}]_2$, respectively. Therefore, the resonance at 1.619 and 2.500 eV are labeled with the configuration of $4s[^2S_{1/2}]4d_{5/2}$ ($J = 2$) and $3d[^2D_{3/2}]8s$ ($J = 2$), respectively. It is known that CI could redistribute the resonance strength among different autoionizing levels. Here, it is found that the strength of the resonance at 2.405 eV is enhanced by over one order of magnitude due to the inclusion of the CI between the $3lnl'$ and $4lnl'$ configurations.

As shown in the lower panel in Fig. 2, the resonance positions and strengths are also well reproduced by the present AUTOSTRUCTURE calculation at collision energy higher than 3 eV. However, the calculated position of the first resonance is about 12% higher than the measurement at around 1.619 eV. In addition, the calculated strength of the resonance at 2.500 eV is about a factor of 2 higher than the measured one. These discrepancies are also caused by the strong mixing among the low-energy resonances as mentioned in the FAC calculation.

In the higher energy range, a very good agreement between the experimental results and the two different theoretical calculations is found as shown in Fig. 3. The series limits from $3s[^2S_{1/2}] \rightarrow 3p[^2P_{1/2}]$ and $3s[^2S_{1/2}] \rightarrow 3p[^2P_{3/2}]$ are clearly observed in the spectrum. In order to show the field-ionization-free electron-ion recombination rate coefficients, the FAC and AUTOSTRUCTURE calculations are performed with $n_{\text{max}} = 300$ and $n_{\text{max}} = 1000$ and indicated with dashed red and dashed-dotted blue curves in the upper and lower panels in Fig. 3, respectively. In addition, the FAC calculation with $n_{\text{cut-off}} = 150$ is presented with a dashed orange curve to show the filed ionization effect at $3pnl$ series limits at around 55 and 70 eV. In order to compare the measured DR rate coefficients with the calculations in more detail, we fitted the resolved peaks in the measured spectrum to extract the resonance energies and strengths at the energy range from 0 to 45 eV. The fitting results of resonance energies and strengths are listed in Tables II and III and compared with the FAC and AUTOSTRUCTURE calculations.

B. Plasma recombination rate coefficients

Temperature dependent plasma recombination rate coefficients (PRRC) are of great importance for plasma modeling and diagnostics. In contrast to the very narrow anisotropic velocity distribution of the electron beam characterized by the $k_B T_\perp$ and $k_B T_\parallel$ in a storage ring experiment, the electrons have a much broader Maxwellian-Boltzmann velocity distribution in astrophysical and fusion plasmas. Thus, the plasma recombination rate coefficient can be obtained by the convolution of DR rate coefficients $\alpha(E)$ with a Maxwell-Boltzmann velocity distribution characterized by the plasma electron temperature T_e as shown below [35]:

$$\alpha(T_e) = \int \alpha(E) f(E, T_e) dE, \tag{10}$$

TABLE II. Comparison of the calculated and measured resonance energies E_d and strengths S_d of $3lnl'$ states.

Intermediate state configuration	E_d(eV)			S_d(10^{-19} eV cm^2)		
	FAC	AUTOS	Exp[b]	FAC	AUTOS	Exp[b]
$3d[^2D_{3/2}]8s$ ($J=1$)	2.090	2.117	2.032 ± 0.009	7.08	12.23	9.5 ± 1.5
$3d[^2D_{3/2}]8s$ ($J=2$)[c]	2.405	1.822	2.500 ± 0.002	62.20	101.01	42.4 ± 1.5
$3d[^2D_{5/2}]8s$ ($J=3$)	4.530	4.568		7.30	12.79	
$3p[^2P_{1/2}]13p_{1/2}$	4.565[a]	4.565[a]		4.38	3.91	
blend	4.543[a]	4.567[a]	4.565 ± 0.003	11.68	16.70	17.8 ± 2.0
$3d[^2D_{3/2}]8p_{1/2}$ ($J=2$)	4.660	4.771		6.36	1.72	
$3d[^2D_{5/2}]8s$ ($J=2$)	4.690	4.599		11.01	4.59	
blend	4.679[a]	4.646[a]	4.709 ± 0.009	17.37	6.31	14.3 ± 1.5
$3d[^2D_{3/2}]8p_{1/2}$ ($J=1$)	4.754	4.837	4.920 ± 0.053	3.88	3.08	2.7 ± 1.5
$3d[^2D_{3/2}]8p_{3/2}$ ($J=2$)	5.206	5.286	5.135 ± 0.013	3.71	1.84	10.9 ± 1.5
$3d[^2D_{3/2}]8p_{3/2}$ ($J=3$)	5.354	5.455		6.83	5.34	
$3p[^2P_{1/2}]13d_{3/2}$	5.384[a]	5.384[a]		7.20	7.44	
Blend	5.369[a]	5.414[a]	5.350 ± 0.020	14.03	12.78	14.5 ± 3.5
$3d[^2D_{3/2}]8p_{3/2}$ ($J=0$)	5.477	5.551	5.460 ± 0.027	1.01	0.86	6.9 ± 2.1
$3p[^2P_{1/2}]13f$	5.838[a]	5.837[a]	5.774 ± 0.017	12.41	12.82	11.1 ± 1.8
$3p[^2P_{1/2}]13g$	5.967[a]	5.966[a]	5.934 ± 0.005	8.09	8.34	8.9 ± 1.8
$3p[^2P_{1/2}]13l$ ($l \geqslant h$)	6.013[a]	6.012[a]	6.060 ± 0.022	32.35	32.25	35.3 ± 3.7
$3d[^2D_{5/2}]8p_{1/2}$ ($J=3, 2$)	7.129[a]	7.265[a]	7.233 ± 0.019	14.57	5.96	8.2 ± 1.5
$3p[^2P_{3/2}]12s$ ($J=1, 2$)	7.465[a]	7.466[a]	7.471 ± 0.026	2.04	1.63	1.89 ± 0.7
$3p[^2P_{3/2}]12p_{1/2}$	8.245[a]	8.247[a]	8.015 ± 0.067	2.20	1.88	2.5 ± 1.7
$3p[^2P_{3/2}]12p_{3/2}$	8.404[a]	8.403[a]	8.415 ± 0.032	3.84	3.48	4.00 ± 2.3
$3d[^2D_{3/2}]8d_{3/2}$	8.596[a]	8.818[a]	8.675 ± 0.015	12.65	12.34	14.5 ± 1.6
$3d[^2D_{3/2}]8d_{5/2}$	8.813[a]	8.822[a]	8.808 ± 0.027	21.07	18.97	19.5 ± 2.1
$3p[^2P_{3/2}]12d$	9.404[a]	9.407[a]	9.340 ± 0.008	8.88	8.98	12.6 ± 1.5
$3p[^2P_{3/2}]12f$	9.979[a]	9.982[a]		18.59	19.07	
$3p[^2P_{3/2}]12g$	10.118[a]	10.143[a]		8.81	13.13	
$3p[^2P_{3/2}]12l$ ($l \geqslant h$)	10.153[a]	10.201[a]		50.09	46.76	
Blend	10.107[a]	10.139[a]	10.162 ± 0.004	77.49	78.97	80.2 ± 1.5
$3d[^2D_{3/2}]8f$	10.720[a]	10.790[a]	10.648 ± 0.017	38.25	36.31	35.0 ± 1.9
$3d[^2D_{5/2}]8d$	11.227[a]	11.129[a]	10.930 ± 0.016	33.13	36.80	34.8 ± 2.0
$3p[^2P_{1/2}]14p$	11.790[a]	11.789[a]	11.532 ± 0.006	1.37	1.24	3.1 ± 2.1
$3p[^2P_{1/2}]14d$	12.545[a]	12.442[a]	12.488 ± 0.566	3.60	2.61	4.9 ± 2.0
$3p[^2P_{1/2}]14l(l \geqslant f)$	12.907[a]	12.905[a]	12.939 ± 1.236	19.42	19.51	22.8 ± 4.1
$3d[^2D_{5/2}]8f$	13.275[a]	13.247[a]	13.153 ± 0.058	25.37	37.79	17.7 ± 5.4
$3d[^2D_{5/2}]8l$ ($l \geqslant g$)	13.568[a]	13.835[a]	13.547 ± 0.028	84.6	82.59	18.6 ± 3.1
$3p[^2P_{3/2}]13p$	17.491[a]	17.492[a]		2.41	2.17	
$3p[^2P_{1/2}]15p$	17.601[a]	17.600[a]		0.76	0.69	
Blend	17.517[a]	17.518[a]	17.600 ± 0.002	3.17	2.86	4.8 ± 1.0
$3p[^2P_{1/2}]15d$	18.131[a]	18.130[a]	18.117 ± 0.027	1.43	1.48	4.4 ± 1.4
$3p[^2P_{3/2}]13d$	18.313[a]	18.315[a]	18.401 ± 0.071	3.64	3.68	2.3 ± 1.0
$3p[^2P_{1/2}]15l$ ($l \geqslant f$)	18.533[a]	18.532[a]	18.691 ± 0.002	8.78	8.72	13.7 ± 1.2
$3p[^2P_{3/2}]13l$ ($l \geqslant f$)	18.930[a]	18.929[a]	18.984 ± 0.057	25.51	25.60	29.1 ± 1.1
$3p[^2P_{1/2}]16l$	23.005[a]	23.047[a]	23.008 ± 0.041	9.53	8.57	6.1 ± 1.2
$3p[^2P_{3/2}]14s$	24.159[a]	24.159[a]	24.201 ± 0.050	0.42	0.35	2.1 ± 1.3
$3p[^2P_{3/2}]14p$	24.715[a]	24.716[a]		1.41	1.28	
$3p[^2P_{3/2}]14d$	25.371[a]	25.372[a]		2.15	2.16	
Blend	25.111[a]	25.128[a]	25.000 ± 0.142	3.56	3.44	2.22 ± 1.1
$3p[^2P_{3/2}]14l$ ($l \geqslant f$)	25.865[a]	25.864[a]	25.785 ± 0.037	20.73	20.60	16.8 ± 1.0
$3p[^2P_{1/2}]17l$	26.821[a]	26.824[a]	26.879 ± 0.001	7.23	7.05	4.6 ± 1.1
$3p[^2P_{1/2}]18l$	30.020[a]	30.020[a]	30.076 ± 0.003	6.10	5.70	6.6 ± 0.9
$3p[^2P_{3/2}]15l$	31.348[a]	31.341[a]	31.382 ± 0.057	16.35	17.64	11.6 ± 0.2
$3p[^2P_{1/2}]19l$	32.739[a]	32.719[a]	32.700 ± 0.037	7.53	4.49	5.7 ± 1.1
$3p[^2P_{1/2}]20l$	35.030[a]	35.030[a]	34.800 ± 0.053	4.19	4.13	3.2 ± 1.0
$3p[^2P_{3/2}]16l$	35.965[a]	35.945[a]	35.884 ± 0.049	12.42	13.77	11.8 ± 0.7
$3p[^2P_{1/2}]21l$	37.015[a]	36.806[a]	37.038 ± 0.562	3.70	3.73	3.5 ± 0.5

TABLE II. (*Continued.*)

Intermediate state configuration	E_d(eV)			$S_d(10^{-19}$ eV cm^2)		
	FAC	AUTOS	Exp[b]	FAC	AUTOS	Exp[b]
$3p[^2P_{1/2}]22l$	38.735[a]	38.734[a]	38.800 ± 0.527	3.31	3.31	7.7 ± 1.5
$3p[^2P_{3/2}]17l$	39.751[a]	39.76[a]	39.7615 ± 0.127	10.60	11.14	10.3 ± 1.2
$3p[^2P_{1/2}]23l$	40.241[a]	40.234[a]	40.235 ± 0.118	3.01	3.02	7.3 ± 3.6
$3p[^2P_{1/2}]24l$	41.551[a]	41.566[a]	41.552 ± 0.010	2.77	2.62	5.3 ± 2.9
$3p[^2P_{1/2}]25l$	42.712[a]	42.711[a]		2.57	2.60	
$3p[^2P_{3/2}]18l$	42.946[a]	42.984[a]		8.96	9.56	
Blend	42.894[a]	42.925[a]	42.883 ± 0.024	11.53	12.16	10.9 ± 1.0
$3p[^2P_{1/2}]26l$	43.742[a]	43.740[a]	43.554 ± 0.098	2.40	2.44	2.6 ± 1.1

[a]Weighted energy: $E_d = \frac{\sum E_d S_d}{\sum S_d}$.
[b]Standard error from the fit at 1 σ confidence level only and the uncertainties from the absolute measurement are not included, the experimentally measured rate coefficients have a systematic uncertainty of about 30%.
[c]The configurations with highest mixing in intermediate coupling.

TABLE III. Comparison of the calculated and measured resonance energies E_d and strengths S_d of $4l4l'$ states:

Intermediate state configuration	E_d(eV)			$S_d(10^{-19}$ eV cm^2)		
	FAC	AUTOS	Exp[b]	FAC	AUTOS	Exp[b]
$4s[^2S_{1/2}]4d_{5/2}\ (J=2)$[c]	1.530	2.476	1.619 ± 0.001	75.21	193.03	75.1 ± 1.5
$4s[^2S_{1/2}]4f_{5/2}\ (J=2)$	8.130	8.138	8.168 ± 0.005	37.85	33.83	42.4 ± 1.5
$4s[^2S_{1/2}]4f_{5/2}\ (J=3)$	8.880	8.885	8.905 ± 0.010	53.93	46.55	64.9 ± 4.6
$4s[^2S_{1/2}]4f_{7/2}\ (J=4)$	9.577	9.597	9.664 ± 0.003	65.71	57.72	73.8 ± 1.6
$4s[^2S_{1/2}]4f_{5/2}\ (J=3)$	9.737	9.852	9.894 ± 0.040	55.78	53.70	54.9 ± 1.6
$4p[^2P_{1/2}]4d_{3/2}(J=2)$	13.926	14.183	14.142 ± 0.059	4.50	4.55	8.2 ± 4.8
$4p[^2P_{1/2}]4d_{5/2}\ (J=3)$	16.337	16.506	16.388 ± 0.001	12.31	8.36	10.2 ± 1.0
$4p[^2P_{1/2}]4d_{3/2}\ (J=1)$	18.466	18.680	18.462 ± 0.003	5.23	4.14	5.3 ± 2.3
$4p[^2P_{3/2}]4d_{5/2}\ (J=4)$	19.112	19.119	19.115 ± 0.003	2.22	2.52	2.7 ± 1.3
$4p[^2P_{3/2}]4d_{3/2}\ (J=2)$	20.038	20.048	19.923 ± 0.001	5.08	3.94	6.4 ± 1.7
$4p[^2P_{3/2}]4d_{3/2}\ (J=0)$	21.802	21.758	21.800 ± 0.024	1.65	1.31	1.7 ± 0.3
$4p[^2P_{3/2}]4d_{3/2}\ (J=1)$	22.054	22.038	22.330 ± 0.039	4.25	3.25	5.4 ± 1.4
$4p[^2P_{3/2}]4d_{5/2}\ (J=3)$	22.444	22.494		4.26	2.98	
$4p[^2P_{3/2}]4d_{5/2}\ (J=2)$	22.502	22.513		5.43	4.00	
Blend	22.476	22.505	22.492 ± 0.077	9.69	6.99	10.1 ± 1.4
$4p[^2P_{3/2}]4d_{5/2}\ (J=1)$	29.088	29.096	29.120 ± 0.015	5.50	4.75	7.4 ± 0.1
$4p[^2P_{3/2}]4d_{3/2}(J=3)$	31.474	32.451		11.87	10.46	
$4p[^2P_{1/2}]4f_{5/2}(J=3)$	32.424	32.743		1.64	1.84	
Blend	31.589	32.495	31.558 ± 0.733	13.51	12.30	9.5 ± 0.8
$4p[^2P_{1/2}]4f_{7/2}(J=4)$	33.180	33.470	33.231 ± 0.422	1.72	1.49	2.6 ± 0.1
$4p[^2P_{3/2}]4f_{5/2}(J=3)$	36.851	37.015		1.69	1.31	
$4p[^2P_{3/2}]4f_{7/2}(J=3)$	37.285	37.460		3.30	1.83	
Blend	37.138	37.278	36.950 ± 0.156	4.99	3.11	3.3 ± 0.1
$4p[^2P_{3/2}]4f_{5/2}(J=4)$	38.374	38.517		5.72	3.83	
$4p[^2P_{3/2}]4f_{7/2}(J=5)$	38.436	38.657		4.86	4.04	
Blend	38.4.2	38.589	38.417 ± 0.042	10.58	7.87	8.9 ± 1.3
$4p[^2P_{3/2}]4f_{5/2}(J=2)$	39.697	40.208		4.52	2.26	
$4p[^2P_{3/2}]4f_{5/2}(J=1)$	40.808	41.194		0.46	0.49	
Blend	39.765	40.258	40.088 ± 0.141	4.92	2.75	4.9 ± 1.0
$4p[^2P_{3/2}]4f_{7/2}(J=2)$	42.274	42.677	42.200 ± 0.072	4.44	4.64	3.7 ± 0.9

[a]Weighted energy: $E_d = \frac{\sum E_d S_d}{\sum S_d}$.
[b]Standard error from the fit at 1 σ confidence level only and the uncertainties from the absolute measurement are not included, the experimentally measured rate coefficients have a systematic uncertainty of about 30%.
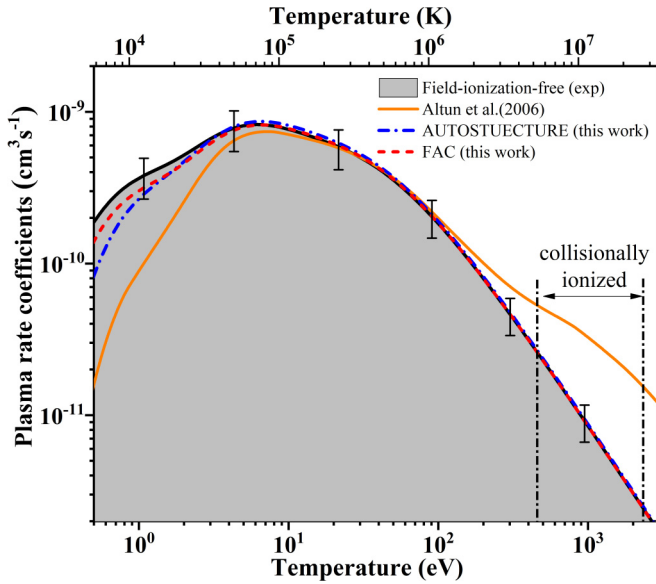[c]The configurations with highest mixing coefficient in intermediate coupling.

FIG. 4. The comparison of the present experimentally derived plasma rate coefficient (black solid curve and gray area) with the FAC (dashed red) and AUTOSTRUCTURE (dashed-dotted blue) results in this work, and the recommended data of Altun *et al.* (2006, orange solid curve). The error bars denote the $\pm 30\%$ experimental uncertainty of the absolute rate coefficient. The approximate temperature ranges where Kr^{25+} is expected to form in collisionally ionized plasmas are indicated by vertical dash-dotted bars and associated arrows [54,55].

where $f(E, T_e)$ is the electron energy distribution, which can be expressed as [3]

$$f(E, T_e) = \frac{2E^{1/2}}{\pi^{1/2}(kT_e)^{3/2}}\exp\left(-\frac{E}{kT_e}\right). \tag{11}$$

Temperature dependent plasma rate coefficients derived from the experimental result and the present theoretical calculations as well as the data from literature are displayed in Fig. 4. However, one has to be aware of the fact that high-n

Rydberg states are easily field ionized in the storage ring DR experiments. In order to obtain the field-ionization-free plasma recombination rate coefficients, the measured DR rate coefficients from 55–57 eV and 68–70 eV were replaced by the corresponding AUTOSTRUCTURE calculated results including the resonances with the free electron captured into the Rydberg levels $n_{\max} = 1000$. The contribution from the resonances with principal quantum number n lager than 1000 was tiny enough to be safely neglected. The experiment is mimicking a steady-state coronal plasma. Altun *et al.* provided DR data relevant to modeling dynamic finite-density plasmas as found in magnetic fusion [38]. At even higher densities, as found in laser produced plasmas, further effects need to be considered [53].

In Fig. 4, the present experimentally derived plasma rate coefficient is compared with the recommended data of Altun *et al.* [34] and with the theoretical results calculated by the FAC and AUTOSTRUCTURE Code in this work. The recommended data of PRRC from Altun *et al.* is presented with an orange solid curve, which is much lower than the experimentally derived PRRC in the temperature range from 0 to 10 eV. However, the present AUTOSTRUCTURE calculated PRRC (dashed-dotted blue) has a good agreement with the experimental one in the whole measured energy range, within the 30% experimental uncertainty. It should be noted that the theoretical calculation of Altun *et al.* also used the AUTOSTRUCTURE code and the configurations considered in the calculation were almost the same as the calculation in the present work. However, Altun *et al.* calculated the DR resonances associated with the $3 \rightarrow 3$ and $3 \rightarrow 4$ core excitations separately. Consequently, there was no mixing between the *3d8s* and *4s4d* configurations. In the present AUTOSTRUCTURE calculation, the necessary mixing between the low lying $\Delta n = 0$ *and* $\Delta n = 1$ DR resonances was included. The difference between FAC calculation and the experimentally derived plasma rate coefficient is less than 20%, which is mainly caused by the unreliable resonance positions and strengths at low energy range in the calculation.

TABLE IV. Fitted parameters of plasma recombination rate coefficients for DR of Kr^{25+} forming Kr^{24+}. The units of c_i and E_i are $cm^{-3}\,s^{-1}\,K^{3/2}$ and eV, respectively. Numbers in the squared brackets are powers of 10. The experimental results are field-ionization free DR plasma rate coefficients as described in the text, the AUTOSTRUCTURE results for $n_{\max} = 1000$ and the FAC results for $n_{\max} = 300$.

No.	Experiment	FAC	AUTOSTUCTURE
c_1	4.470[−9]	1.736[−1]	1.721[−7]
c_2	1.330[−9]	7.490[−7]	5.521[−8]
c_3	1.580[−7]	5.430[−8]	2.027[−9]
c_4	0.149[0]	6.130[1]	7.976[−9]
c_5	4.610[−8]	1.990[−7]	1.741[8]
c_6	4.400[−8]	2.430[−9]	1.897[10]
c_7	2.199[4]	7.895[−2]	4.972[−8]
E_1	3.570[−4]	7.626[0]	5.150[−3]
E_2	1.300[−4]	11.056[0]	2.560[−3]
E_3	4.970[−3]	8.600[−4]	1.827[−4]
E_4	1.120[2]	2.004[2]	5.016[−4]
E_5	2.200[−3]	3.910[−3]	2.805[11]
E_6	8.700[−4]	1.750[−4]	4.386[11]
E_7	7.170[11]	2.483[1]	9.557[−4]

In the temperature range 10–70 eV, the recommended data from Altun *et al.* agree within 10% with the experimentally derived plasma rate coefficient. The FAC and AUTOSTRUCTURE calculated plasma rate coefficients in the present work agree with the experimental result within 5%. One has to note that the present measurement leaves out many of the $3s \rightarrow 3d$ and most of the $\Delta n = 1$ resonances, while they were included in calculations of Altun *et al.* [34]. Consequently, the experimentally derived plasma rate coefficients in the present work can be used as a benchmark for the low temperature up to $\sim 1 \times 10^6$ K, and the calculated data by Altun *et al.* [34] provide reliable plasma rate coefficients at high temperature range above 2×10^6 K. The temperature ranges associated with collisionally ionized plasmas in which Kr^{25+} concentration is higher than 10% of its maximum abundance are indicated in Fig. 4. In order to facilitate the use of our data in astrophysics and fusion physics modeling, the present experimentally derived plasma rate coefficients have been parameterized. The fitting function we have used is displayed below:

$$\alpha(T_e) = T_e^{-3/2} \sum_i^n c_i \exp\left(-\frac{E_i}{kT_e}\right). \qquad (12)$$

The resulting parameters of c_i and E_i are listed in Table IV. The fitted curves reproduce the experimental plasma rate coefficients within 2% at $\sim 10^4$ K and 1% at $\sim 1 \times 10^6$ K. It should be noted that the plasma rate coefficients are dominated by the $\Delta n = 1$ DR resonances at temperatures over 10^6 K and the fitting parameters in Ref. [34] should be used when modeling collisionally ionized plasmas.

V. CONCLUSIONS

Electron-ion recombination rate coefficients of Na-like Kr^{25+} forming into Mg-like Kr^{24+} were derived from a measurement performed by employing the electron-ion merged-beams method at the cooler storage ring CSRm. No previous experimental results are available for this ion. The experimentally observed DR resonances associated with $\Delta n = 0$ and $\Delta n = 1$ over the energy range from 0 to 70 eV are investigated and identified by comparison with the theoretical calculations using FAC and AUTOSTRUCTURE package. The comparison of the experimental results and the theoretical calculations indicate that the 3–4 core excitation is very strong for DR process of Kr^{25+} at even very low energy range and cannot be neglected. A very good agreement has been achieved between the experimental results and the theoretical calculations by considering strong mixing among the low-energy resonances in both calculations.

A reliable plasma recombination rate coefficients in the low temperature up to medium temperature range was deduced from the measurement in this work, which was then compared with the presently calculated results as well as the data from literature. The present experimental result yields a more precise plasma rate coefficients at the low temperature range up to $\sim 1 \times 10^6$ K and the calculated data by Altun *et al.* [34] provide reliable plasma rate coefficients at high temperature range above 2×10^6 K. The experimentally derived and theoretically calculated plasma rate coefficients at both photoionized- and collision-ionized zones show a good agreement within experimental uncertainty. Our experimental data, together with the theoretical calculations thus provide a benchmark for Kr^{25+} recombination data used in plasma modeling at low temperature.

[1] A. Burgess, Astrophys. J. **139**, 776 (1964).

[2] A. H. Gabriel, Mon. Not. R. Astron. Soc. **160**, 99 (1972).

[3] I. I. Sobel'man, L. A. Vainshtein, and E. A. Yukov, in *Excitation of Atoms and Broadening of Spectral Lines* (Springer, Berlin, 1995), p. 237.

[4] A. Müller, in *Adv. At. Mol. Opt. Phys.*, edited by E. Arimondo, P. R. Berman, and C. C. Lin (Academic Press, New York, 2008), p. 293.

[5] D. Bernhardt *et al.*, Phys. Rev. A **91**, 012710 (2015).

[6] S. Schippers, Nucl. Instrum. Methods Phys. Res. Sect. B **267**, 192 (2009).

[7] D. Bernhardt *et al.*, Phys. Rev. A **83**, 020701(R) (2011).

[8] O. Renner and F. B. Rosmej, Matter Radiat. Extremes **4**, 024201 (2019).

[9] E. Galtier, F. B. Rosmej, T. Dzelzainis, D. Riley, F. Y. Khattak, P. Heimann, R. W. Lee, A. J. Nelson, S. M. Vinko, T. Whitcher *et al.*, Phys. Rev. Lett. **106**, 164801 (2011).

[10] F. Rosmej and J. Abdallah Jr, Phys. Lett. A **245**, 548 (1998).

[11] F. Rosmej, R. Dachicourt, B. Deschaud, D. Khaghani, M. Dozières, M. Šmíd, and O. Renner, J. Phys. B: At. Mol. Opt. Phys. **48**, 224005 (2015).

[12] J. Rice *et al.*, J. Phys. B: At. Mol. Opt. Phys. **51**, 035702 (2018).

[13] H. R. Griem, *Principles of Plasma Spectroscopy* (Cambridge University Press, Cambridge, 1997), Cambridge Monographs on Plasma Physics.

[14] P. Bryans, H. Kreckel, E. Roueff, V. Wakelam, and D. W. Savin, Astrophys. J. **694**, 286 (2009).

[15] N. R. Badnell, J. Phys.: Conf. Ser. **88**, 012070 (2007).

[16] S. Schippers, J. Phys.: Conf. Ser. **163**, 012001 (2009).

[17] S. Schippers, Nucl. Instrum. Methods. Phys. Res. Sect. B. **350**, 61 (2015).

[18] C. Brandau, C. Kozhuharov, M. Lestinsky, A. Müller, S. Schippers, and T. Stöhlker, Phys. Scr. **2015**, 014022 (2015).

[19] R. Schuch and S. Böhm, J. Phys. Conf. Ser. **88**, 012002 (2007).

[20] Z. K. Huang *et al.*, Phys. Scr. **2015**, 014023 (2015).

[21] C. Brandau and C. Kozhuharov, in *Atomic Processes in Basic and Applied Physics*, edited by V. Shevelko and H. Tawara (Springer, Berlin, Heidelberg, 2012), p. 283.

[22] K. Widmann, P. Beiersdorfer, V. Decaux, S. Elliott, D. Knapp, A. Osterheld, M. Bitter, and A. Smith, Rev. Sci. Instrum. **66**, 761 (1995).

[23] P. Beiersdorfer, J. Clementson, K. Widmann, M. Bitter, K. W. Hill, D. Johnson, R. Barnsley, H. K. Chung, and U. I. Safronova, AIP Conf. Proc. **1811**, 190001 (2017).

[24] E. B. Saloman, J. Phys. Chem. Ref. Data **36**, 215 (2007).

[25] E. W. Schmidt *et al.*, Phys. Rev. A **76**, 032717 (2007).

[26] I. Orban, S. Bohm, and R. Schuch, Astrophys. J. **694**, 354 (2009).

[27] J. Linkemann *et al.*, Nucl. Instrum. Methods Phys. Res., Sect. B **98**, 154 (1995).

[28] M. Fogle, N. Eklow, E. Lindroth, T. Mohamed, R. Schuch, and M. Tokman, J. Phys. B **36**, 2563 (2003).

[29] M. Fogle, N. R. Badnell, N. Eklöw, T. Mohamed, and R. Schuch, Astron. Astrophys. **409**, 781 (2003).

[30] M. Gu, Astrophys. J. **590**, 1131 (2003).

[31] M. F. Gu, Can. J. Phys. **86**, 675 (2008).

[32] N. R. Badnell, Comput. Phys. Commun. **182**, 1528 (2011).

[33] C. Brandau *et al.*, Phys. Scr. **1999**, 318 (1999).

[34] Z. Altun, A. Yumak, N. R. Badnell, S. D. Loch, and M. S. Pindzola, Astron. Astrophys. **447**, 1165 (2006).

[35] R. D. Cowan, *The Theory of Atomic Structure and Spectra* (University of California Press, Berkeley, 1981), Vol. 3.

[36] R. Si, X. L. Guo, J. Yan, C. Y. Li, S. Li, M. Huang, C. Y. Chen, Y. S. Wang, and Y. M. Zou, J. Quant. Spectrosc. Radiat. Transfer **163**, 7 (2015).

[37] R. Si, X. L. Guo, J. Yan, C. Y. Li, S. Li, M. Huang, C. Y. Chen, and Y. M. Zou, J. Phys. B: At. Mol. Opt. Phys. **48**, 175004 (2015).

[38] N. R. Badnell *et al.*, Astron. Astrophys. **406**, 1151 (2003).

[39] D. W. Savin *et al.*, Astrophys. J. Suppl. Ser. **147**, 421 (2003).

[40] D. W. Savin *et al.*, Astrophys. J. **642**, 1275 (2006).

[41] G. Kilgus, D. Habs, D. Schwalm, A. Wolf, N. R. Badnell, and A. Müller, Phys. Rev. A **46**, 5730 (1992).

[42] Z. K. Huang *et al.*, Astrophys. J. Suppl. Ser. **235**, 2 (2018).

[43] S.-X. Wang *et al.* Astron. Astrophys. **627**, A171 (2019).

[44] H. W. Zhao, L. T. Sun, J. W. Guo, W. Lu, D. Z. Xie, D. Hitz, X. Z. Zhang, and Y. Yang, Phys. Rev. Spec. Top. Accel. Beams **20**, 094801 (2017).

[45] W. Q. Wen *et al.* Nucl. Instrum. Methods. Phys. Res. Sect. B **317**, 731 (2013).

[46] J. X. Wu *et al.*, Nucl. Instrum. Methods. Phys. Res. Sect. B **317**, 623 (2013).

[47] H. A. Bethe and E. E. Salpeter, *Quantum Mechanics of One and Two Electron Atoms* (Springer, Berlin, 1957), p. 88.

[48] N. Khan *et al.*, Chin. Phys. B **29**, 033401 (2020).

[49] D. R. DeWitt, R. Schuch, H. Gao, W. Zong, S. Asp, C. Biedermann, M. H. Chen, and N. R. Badnell, Phys. Rev. A **53**, 2327 (1996).

[50] M. Fogle, N. Badnell, P. Glans, S. Loch, S. Madzunkov, S. A. Abdel-Naby, M. Pindzola, and R. Schuch, Astron. Astrophys. **442**, 757 (2005).

[51] H. Gao, R. Schuch, W. Zong, E. Justiniano, D. R. DeWitt, H. Lebius, and W. Spies, J. Phys. B: At. Mol. Opt. Phys. **30**, L499 (1997).

[52] K. B. Fournier, A. Y. Faenov, T. A. Pikuz, A. I. Magunov, I. Y. Skobelev, F. Flora, S. Bollanti, P. D. Lazzaro, D. Murra, V. S. Belyaev *et al.*, Phys. Rev. E **70**, 016406 (2004).

[53] F. B. Rosmej *et al.*, J. Phys. B: At. Mol. Opt. Phys. **31**, L921 (1998).

[54] T. Kallman and M. Bautista, Astrophys. J. Suppl. Ser. **133**, 221 (2001).

[55] P. Bryans, E. Landi, and D. W. Savin, Astrophys. J. **691**, 1540 (2009).